frontiers | Frontiers in Electronics

ORIGINAL RESEARCH
published: 01 July 2022
doi: 10.3389/felec.2022.906689

Detection of Atrial Fibrillation in Compressively Sensed Electrocardiogram for Remote Monitoring

Mohamed Abdelazez, Sreeraman Rajan and Adrian D. C. Chan*

Systems and Computer Engineering, Carleton University, Ottawa, ON, Canada

The objective of this paper is to develop an optimized system to detect Atrial Fibrillation (AF) in compressively sensed electrocardiogram (ECG) for long-term remote patient monitoring. A three-stage system was developed to 1) reject ECG of poor signal quality, 2) detect AF in compressively sensed ECG, and 3) detect AF in selectively reconstructed ECG. The Long-Term AF Database (LTAFDB), sampled at 128 Hz using a 12-bit ADC with a range of 20 mV, was used to validate the system. The LTAFDB had 83,315 normal and 82,435 AF rhythm 30 s ECG segments. Clean ECG from the LTAFDB was artificially contaminated with motion artifact to achieve −12 to 12 dB Signal-to-Noise Ratio (SNR) in steps of 3 dB. The contaminated ECG was compressively sensed at 50% and 75% compression ratio (CR). The system was evaluated using average precision (AP), the area under the curve (AUC) of the receiver operator characteristic curve, and the F1 score. The system was optimized to maximize the AP and minimize ECG rejection and reconstruction ratios. The optimized system for 50% CR had 0.72 AP, 0.63 AUC, and 0.58 F1 score, 0.38 rejection ratio, and 0.38 reconstruction ratio. The optimized system for 75% CR had 0.72 AP, 0.63 AUC, and 0.59 F1 score, 0.40 rejection ratio, and 0.35 reconstruction ratio. Challenges for long-term AF monitoring are the short battery life of monitors and the high false alarm rate due to artifacts. The proposed system improves the short battery life through compressive sensing while reducing false alarms (high AP) and ECG reconstruction (low reconstruction ratio).

Keywords: signal quality assessment, remote healthcare, compressive sensing, electrocardiogram, machine learning, atrial fibrillation

OPEN ACCESS

Edited by:
Hugo F. Posada-Quintero, University of Connecticut, United States

Reviewed by:
Syed Bashar, Johns Hopkins University, United States
Shirin Hajeb, University of Connecticut, United States

****Correspondence:***
Mohamed Abdelazez
mohamedabdelazez@cmail.carleton.ca

Specialty section:
This article was submitted to Wearable Electronics, a section of the journal Frontiers in Electronics

Received: *28 March 2022*
Accepted: *06 June 2022*
Published: *01 July 2022*

Citation:
Abdelazez M, Rajan S and Chan ADC (2022) Detection of Atrial Fibrillation in Compressively Sensed Electrocardiogram for Remote Monitoring. Front. Electron. 3:906689. doi: 10.3389/felec.2022.906689

1 INTRODUCTION

Atrial Fibrillation (AF) is a cardiovascular disease that arises from the uncoordinated activation of the atria (January et al., 2014). AF can lead to severe complications, including a 2-, 3-, and 5-fold increase in risk in mortality and dementia, heart failure, and stroke, respectively (Ott et al., 1997; Kannel et al., 1998; Stewart et al., 2002; Alonso et al., 2009). Additionally, patients with AF are twice as likely to be hospitalized and three times more likely to be readmitted to a hospital than patients without AF (January et al., 2014). AF patients may not exhibit symptoms (silent AF) and can experience short (< 7 days), long (> 7 days), and persistent (> 12 months) AF episodes (Go et al., 2014; January et al., 2014).

Cardiac activity can be monitored for AF using photoplethysmography (PPG), video-based contactless monitors, and electrocardiogram (ECG) (Couderc et al., 2015; Han et al., 2020; Lazaro et al., 2020; Pereira et al., 2020; Bashar et al., 2021). PPG is typically collected using optical-based wearable devices, such as commercially available smart watches, which provides an accessible approach to monitoring AF. Couderc et al. (2015) suggested using machine learning based approach to detect AF from PPG achieving sensitivity, specificity, positive predicted value, negative predicted value, and accuracy of 92%, 96%, 85%, 98%, and 95%, respectively. Han et al. (2020) wrote a review of the techniques to detect AF using PPG with the referenced techniques achieving accuracy, sensitivity, and specificity of 99.9, 99.9, and 99.8%, responsively. Additionally, Han et al. (2020) have identified that one of the challenges of using PPG for AF detection is its susceptibility to motion artifact, where a PPG corrupted with motion artifact resembles AF such that monitoring for AF during ambulation may not feasible. Another optical-based approach is using a contactless video monitor; variation in the skin color due to changes in blood flow can be used to monitor the heartbeat (Couderc et al., 2015). These techniques require the participant to be in the camera's field of view limiting their application to stationary patients. ECG recordings are typically used to detect and diagnose AF and are considered the clinical gold standard (Kumar Sahoo et al., 2011). ECG is typically recoded using electrodes placed on the patient's torso, however armband electrodes have been recently suggested (Lazaro et al., 2020). ECG is the focus of this paper since it is the clinical gold standard for monitoring and detecting AF (Podd et al., 2016). AF can have an irregular heart rate, an absent P-wave, and/or an irregular atrial activity (January et al., 2014). Since AF episodes can be silent, short, and occur sporadically, long-term remote patient monitoring of ECG is beneficial. For instance, a study showed that the AF detection rate increased from 6.2% at the end of 30 days of monitoring to 40% at 30 months (Reiffel et al., 2017).

Remote mobile ECG monitoring is often employed to allow individuals to move about during monitoring. A Holter monitor is a commonly used wearable ECG monitor that will record the ECG over a specific period (e.g., 24–72 h), and then a clinician will download the ECG from the monitor and analyze it offline for any abnormalities (Kusumoto Fred et al., 2019), but AF detection may require months of ECG monitoring; therefore, ECG will need to be regularly downloaded for frequent analysis. However, regularly downloading the ECG could be inconvenient for the patients as they may need to regularly visit a clinic or use specialized devices (Medtronic, 2020). As such, a wireless ECG wearable monitor and automated analysis of ECG can facilitate long-term monitoring and detection of AF; however, the short battery life of wearable ECG monitors is a challenge (Serhani et al., 2020). Additionally, remote mobile monitoring has been shown to introduce contaminants in the ECG, which increases the rate of false alarms in AF detection and, in turn, can render long-term ECG monitors unusable (Taji et al., 2018). Signal quality analysis (SQA) during long-term mobile monitoring can be used to identify ECG of acceptable quality for further analysis while rejecting unacceptable ECG to reduce false alarms.

Compressive sensing (CS), introduced in 2006, is used to compress signals at the sensing stage (Candès et al., 2006). CS is a computationally simple technique that can achieve high compression ratios (CRs) and reduce the battery consumption of healthcare monitors by up to 15.4% (Al Disi et al., 2018). As such, CS could be performed on the wearable remote mobile ECG monitor to overcome the short battery life challenge. However, reconstructing compressively sensed ECG is an ill-posed problem and a computationally intensive operation (Poian et al., 2016). Therefore, SQA and detection of AF in compressively sensed ECG are warranted to avoid needless signal reconstruction.

The contribution of this paper is the development of a novel system that assesses the signal quality and detects AF in compressively sensed ECG, thereby minimizing the need to reconstruct the compressed ECG. In this paper, the system's performance is assessed, the impact of contaminated ECG on AF detection is explored, and optimization of the system to maximize performance, reduce computational complexity, and reduce false alarms is presented. The remainder of this paper is divided into six sections. **Section 2** provides literature review on SQA and AF detection. **Section 3** provides an overview of the proposed system. **Section 4** describes the methodology, including the data, the compression algorithm, and the training and testing procedure. **Sections 5**, **6** describe and discuss the results, respectively. Finally, **Section 7** provides the conclusions and future work.

2 LITERATURE REVIEW

2.1 Atrial Fibrillation Detection

AF detection algorithms generally consist of two major steps: 1) feature extraction and 2) classification. Deep learning algorithms can combine the feature extraction and classification steps (Andersen et al., 2019; Mousavi et al., 2019; Sun et al., 2020; Pokaprakarn et al., 2021). Features for AF detection may reflect the changes in the P-wave and R-R interval associated with AF (Rizwan et al., 2020). F-wave analysis can also be performed for AF detection; however, isolation of F-wave and extraction of its features are challenging due to its low amplitude (Rizwan et al., 2020). Other features can highlight AF but are extracted without identifying ECG fiducial points (Asgari et al., 2015; Kora and Sri Rama Krishna, 2016; Lim et al., 2016). These non-fidicual-based features include statistical- and transform-based features (Hussein et al., 2018; Marinho et al., 2019; Nascimento et al., 2020; Rizwan et al., 2020).

There have been few studies exploring the detection of AF in compressively sensed ECG. Poian et al. (2018) proposed a modified matched filter technique to detect heartbeats in compressively sensed ECG. The technique successfully located the heartbeats; however, the technique required a template of each patient's heartbeat, requiring regular updating. Poian et al. (2017) utilized the matched filtering technique to detect AF in compressively sensed ECG by locating the heartbeats, extracting RRI features, and using a support vector machine to differentiate ECG with AF from normal ECG. Cheng et al. (2020), Zhang et al. (2020) proposed using deep learning to detect AF in compressively sensed ECG.

Detecting ECG fiducial points can be challenging for different compression matrices and higher compression levels. The AF

detection system proposed in this paper detects AF in compressively sensed ECG using a non-fiducial-based features approach, introduced in (Abdelazez et al., 2021). With clean ECG, this approach achieved an average precision of 0.90, 0.91, and 0.91 at 50%, 75%, and 95% compression, respectively (Abdelazez et al., 2021). Long-term AF monitoring may take place while the patient is ambulating contaminating the ECG. SQA would identify the quality of the ECG to reduce false AF detections.

2.2 Signal Quality Analysis

SQA can be broken into four categories (Fraser et al., 2014): 1) detection, recognizing the presence of a contaminant in the ECG; 2) identification, determining the type of the contaminant; 3) quantification, estimating the level of contamination or equivalently assessing the quality of the ECG; and 4) mitigation, removing/reducing the contaminant. For quantification, the quality of ECG can be represented using a Signal Quality Index (SQI), which can be on a continuous scale [e.g., signal-to-noise ratio (SNR)] or a discrete scale (e.g., unacceptable, intermediate, or acceptable). Detection can be considered an abstraction of quantification, where a threshold of acceptability is applied to the SQI. Different applications will have different thresholds of acceptability. For example, heart rate (HR) detection, an application tolerant to high contamination levels, would likely have a higher threshold of acceptability than AF detection, a process that is adversely affected by even low levels of contaminants.

Quality analysis of ECG consists of two steps: 1) features extraction and 2) quality classification/regression. The features can be fiducial-based or non-fiducial-based (Satija et al., 2018). Fiducial-based features require identifying fiducial points in the ECG (e.g., R-peak). Non-fiducial-based features are extracted directly from the ECG or following a transformation (e.g., Wavelet transform). In addition, the cross-correlation between ECG leads and ECG lead autocorrelation have also been used as features (Satija et al., 2018). A review of SQA techniques can be found in (Satija et al., 2018).

SQI for compressively sensed ECG has been scarcely explored. Liu et al. (2021) proposed a discrete SQI that used non-fiducial-based features (energy and wavelet entropy) to classify compressively sensed ECG as either acceptable or unacceptable, which should be considered SQA detection rather than quantification. The SQI had a maximum accuracy of 90.43% when tested on the Physionet/CinC Challenge 2011 Database, compressed at 50% using a Gaussian matrix.

The AF detection system proposed in this paper uses an SQI for compressively sensed ECG that we introduced in (Abdelazez et al., 2022). Our SQI estimates the SNR on a continuous scale. Unlike (Liu et al., 2021), this allows different thresholds of acceptability to be chosen for different applications.

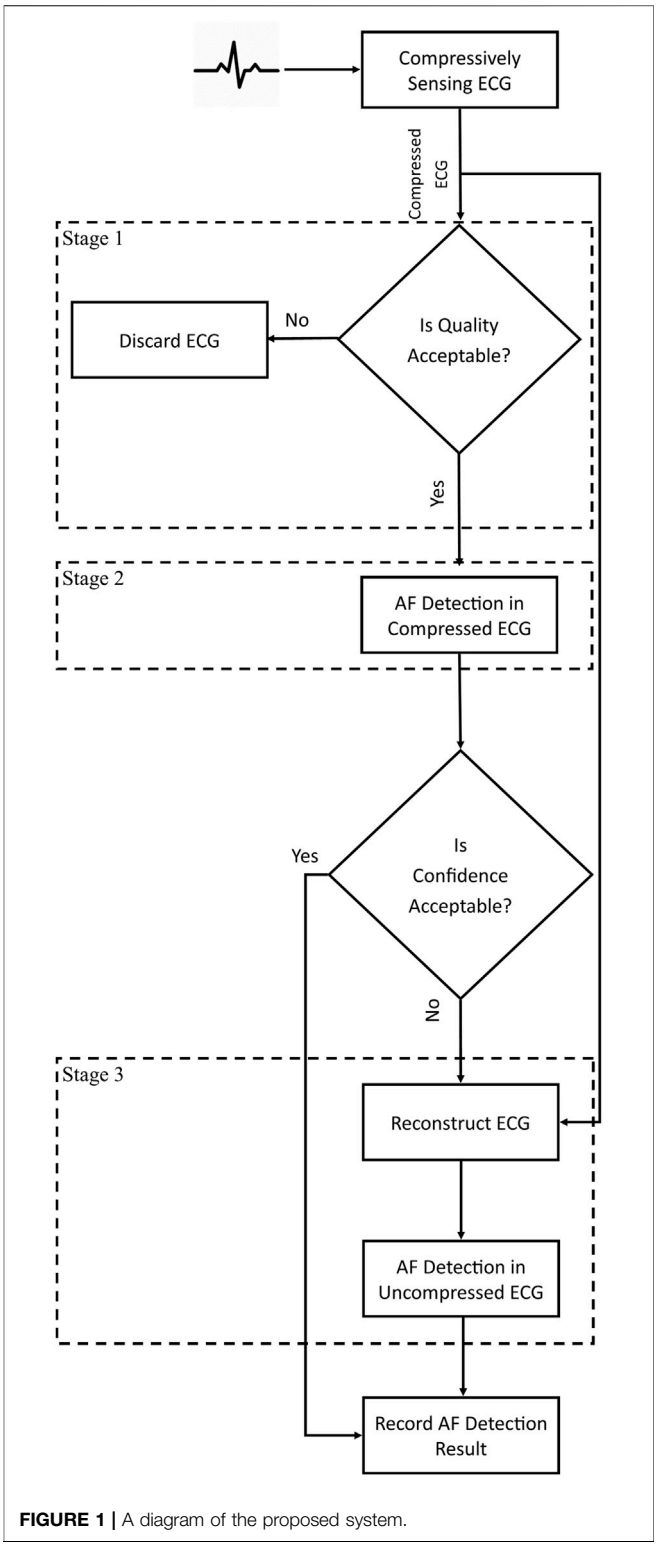

FIGURE 1 | A diagram of the proposed system.

3 PROPOSED ATRIAL FIBRILLATION DETECTION SYSTEM

The proposed system is comprised of three stages (**Figure 1**). Stage 1 uses an SQI to determine the quality of the compressively sensed ECG. If the quality is unacceptable, the ECG is discarded to avoid false alarms (i.e., false positives) caused by contaminants. ECG of acceptable quality is processed by Stage 2, which detects AF in the compressively sensed ECG and provides a confidence score for each decision. If the Stage 2 confidence score of AF

detection is unacceptable, Stage 3 reconstructs the ECG, and AF detection is conducted again but on the uncompressed ECG. Stage 3 aims to improve the true alarm rate (i.e., true positives) of the AF detection system while minimizing the computational costs by selectively reconstructing the ECG.

3.1 Stage 1—Signal Quality Index

Contaminated ECG could lead to false alarms, and Stage 1 is intended to reject low-quality ECG to reduce the alarms (i.e., reduce false positives). We previously introduced the SQI used by the proposed system in (Abdelazez et al., 2022). The SQI uses a machine learning approach with feature extraction and regression to estimate the SNR on a continuous scale. There are two non-fiducial-based features: 1) the ratio of the standard deviation (SD) of the amplitudes in an ECG segment (a segment length of 30 s was used in this paper) and the amplitudes of clean ECG, and 2) the Wasserstein distance between the distributions of the amplitudes of an ECG segment and the amplitudes of clean ECG. The distributions are extracted by binning the values of the ECG amplitude in a segment using Scott's rule, defined in (**Eq. 1**) (Scott, 2011).

$$\mathbf{h} = \frac{\mathbf{3.49} * \hat{\boldsymbol{\sigma}}}{\sqrt[3]{\mathbf{n}}} \tag{1}$$

where n is the number of samples in the ECG, $\hat{\sigma}$ is SD of the ECG amplitude, and h is the width of the bin. The Wasserstein distance (also known as the Earth Mover's Distance) is defined in (**Eq. 2**) (Villani, 2009).

$$\mathbf{W}(\mathbf{g},\mathbf{v}): = \min_{\substack{(\mathbf{X},\mathbf{Y}) \\ \mathbf{law}(\mathbf{X})=\mathbf{g} \\ \mathbf{law}(\mathbf{Y})=\mathbf{v}}} \mathbf{E}\|\mathbf{X}-\mathbf{Y}\|_1 \tag{2}$$

where g is the distribution of the ECG segment's amplitudes, v is the distribution of the clean ECG's amplitudes, $\|\ \|_1$ is the L1 norm, and X and Y are random variables with the same distributions as g and v, respectively, as indicated by the law of large numbers (law).

Regression is performed using a random forest (RF), with the hyperparameters (number of trees and minimum ratio of samples in a leaf) optimized using Bayesian optimization (34). The optimized number of trees were 79, 65, and 51 trees, and the minimum optimized ratio of samples in a leaf were 0.00087, 0.00101, and 0.00100 for the uncompressed, 50% compressed, and 75% compressed ECG, respectively.

3.2 Stage 2—Detection of Atrial Fibrillation in Compressively Sensed Electrocardiogram

We previously introduced the machine learning approach for AF detection in compressively sensed ECG (Abdelazez et al., 2021). The features are non-fiducial based: statistical features (median, skewness, and range), EMD, Discrete Cosine Transform (DCT), and Discrete Wavelet Transform (DWT). The third and fourth Intrinsic Mode Functions (IMF) are extracted using EMD, as they have been demonstrated to highlight AF features in the ECG (Maji et al., 2013). The mean, skewness, and kurtosis are extracted as features from each IMF. The DCT has been shown to capture the energy levels of the components of the ECG. Energy levels of the components of ECG with and without AF are different (Martis et al., 2014). The median, skewness, kurtosis, and entropy are extracted as features from the DCT coefficients. DWT has been used extensively to analyze, denoise, and compress ECG. The variable scaling of the DWT highlights transient and non-stationary components of the ECG that can identify the presence of AF. The ECG is decomposed to the fourth level using "demy" as the mother wavelet. The mean, median, skewness, and kurtosis are extracted as features from the approximation and detail coefficients generated by the decomposition operation. Feature selection and the final elected features are described in (Abdelazez et al., 2021). 13, 15, and 17 features were selected for uncompressed, 50% compressed, and 75% compressed ECG, respectively.

An RF is used to classify an ECG segment as normal or AF. The RF hyperparameters were optimized using a grid search, resulting in 50 trees, two minimum samples to split, one minimum sample in a leaf, square root of the number of features, and unlimited depth (Abdelazez et al., 2021). These hyperparameters were common across all CRs and the uncompressed ECG.

A confidence score is associated with the classification result, which is the fraction of trees that classified the ECG segment as AF. The confidence score ranges from 0 to 1. A confidence score that approaches one indicates an ECG segment classified as AF with high confidence. A confidence score that approaches 0 indicates an ECG segment classified as normal with high confidence. Confidence scores around 0.5 indicate low confidence in the classification result.

3.3 Stage 3—Detection of Atrial Fibrillation in Electrocardiogram Following Reconstruction

If Stage 2 generates a classification with low confidence, then the ECG segment is reconstructed, and AF detection is performed again on the reconstructed ECG segment. By reconstructing ECG segments with low Stage 2 confidence, Stage 3 is intended to improve the true alarms (i.e., true positives). We previously introduced this approach of selective reconstruction in (Abdelazez et al., 2020), which improved the precision by 3%–4% compared to only performing AF detection in the compressed domain (i.e., Stage 2 without Stage 3). ECG reconstruction is performed using the SL0 algorithm previously used to reconstruct ECG successfully (Mohimani et al., 2009; Mitra et al., 2020). In addition to the sensing matrix, the SL0 requires a sparsifying matrix. A DCT dictionary was provided as the sparsifying matrix, as ECG is sparse in the DCT domain (Mitra et al., 2020).

The fiducial points, specifically the R-wave, can be readily located in the reconstructed ECG; therefore, a fiducial-based AF detection, using RRI features, is employed. An online implementation of the Pan-Tompkins algorithm is used to

locate the R waves (Pan and Tompkins, 1985; Sedghamiz, 2014). First, RRIs are extracted in each ECG segment, and then the following features are extracted: 1) minimum RRI; 2) max RRI; 3) standard deviation of RRI; 4) median of RRI; 5) mean of RRI; 6) the percentage of RRIs less than 50 ms; 7) power of RRIs in the segment; and 8) SampEn of RRIs in segment (Qiao Li et al., 2016). Finally, an RF with the same hyperparameters as stage 2 is used to classify the ECG segment as normal or AF.

4 MATERIALS AND METHODS

4.1 Data

The Long-Term Atrial Fibrillation Database (LTAFDB), available on Physionet, was used to evaluate the proposed system (Goldberger et al., 2000; Petrutiu et al., 2007). There were 84 approximately 24-h records of two-channel ECG collected from 84 subjects in the LTAFDB. ECG was collected at 128 Hz using a 12-bit ADC with a range of 20 mV. The LTAFDB contained annotations of the location of the R-waves and the rhythm type. Only the first channel of ECG and normal rhythm (N) and AF annotations were used in this paper.

To compare the proposed Stage 2 with the literature, Physionet's MIT-BIT Atrial Fibrillation Database (AFDB) was used (Moody, 1983; Goldberger et al., 2000). The database had 21 records that were approximately 10 h sampled at 250 Hz using a 12-bit ADC with a range of 20 mV. Only the first channel of the ECG with N and AF annotations was used.

Each record was preprocessed using a second-order zero-phase Butterworth band-pass filter with a lower cut-off of 0.67 Hz (Kligfield et al., 2007) and an upper cut-off of 25 Hz. The 25 Hz upper cut-off was chosen as the information of AF contained in the F-wave, P-wave, and the R-wave is below 20 Hz (Lin, 2008). Records were then segmented into 30 s non-overlapping segments. Segments that had an SNR above 3 dB, based on the SQI developed in (Quesnel et al., 2014; Abdelazez et al., 2017), were chosen for further analysis. The 3 dB threshold was based on previous studies showing that an AF detector's performance decreased below this threshold (Taji et al., 2018). Additionally, segments with biologically impossible heartrate (< 16 and > 220 beats per minute) were excluded from further analysis. There were 83,315 N and 82,435 AF LTAFDB segments and 14,949 N and 7,905 AF AFDB segments available for further processing.

4.2 Contaminating Electrocardiogram

ECG segments were artificially contaminated using simulated motion artifacts generated using an autoregressive model (Farago and Chan, 2020). Unfortunately, motion artifact overlaps with the ECG in both time and frequency domain, making it challenging to remove. However, other contaminants, such as baseline wandering, muscle artifacts, and high-frequency noise can be easily filtered out.

ECG segments were contaminated to achieve a preset SNR from −12 to 24 dB, in steps of 6 dB. This SNR range was chosen based on the range used in the MIT-BIH Noise Stress Test Database (Moody et al., 1984). The Physionet's Noise Stress Test function SNR definition (Moody et al., 1984) was used for the preset SNR. It should be noted; an 18 dB SNR as defined by Physionet's Noise Stress Test (NST) function is approximately equal to a 3 dB SNR as defined by the SQI used in **Section 4.1** to select segments for further processing. The NST function procedure to contaminate the ECG segments is discussed in (Abdelazez et al., 2022). Following contamination, 916,465 N and 906,785 AF LTAFDB segments were available for further processing.

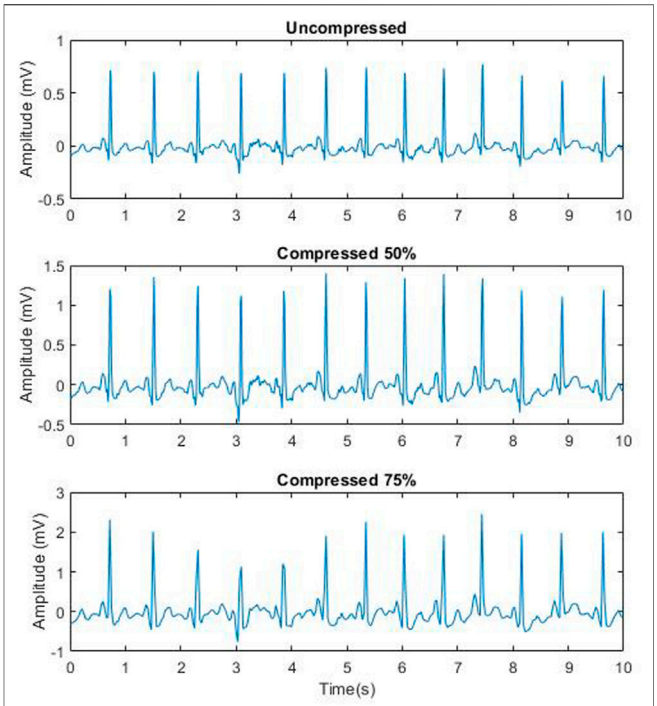

FIGURE 2 | A sample 10 s segment of record five from LTAFDB that is uncompressed (Top), 50% compressed (middle) and 75% compressed (bottom).

4.3 Compressively Sensing Electrocardiogram

Following contamination, each ECG segment was compressively sensed. Compressive sensing (CS) utilizes the sparsity of the ECG to compress it such that the ECG has K-sparse representation in a basis Ψ if its transform, α, contains at most K significant samples (Donoho, 2006). It has been demonstrated that ECG is a sparse signal and that CS can be applied to it successfully (Mitra et al., 2020). The compression operation is described in (**Eq. 3**).

$$\boldsymbol{y} = \boldsymbol{\Phi x} \tag{3}$$

where x is the ECG segment of size $Z \times 1$, Φ is the sensing matrix of size $M \times Z$, and y is the compressively sensed ECG of size $M \times 1$. Previous work successfully demonstrated AF detection in compressively sensed ECG using the deterministic binary block diagonal (DBBD) sensing matrix (Abdelazez et al.,

2021). The DBBD is used in this work, and a sample DBBD matrix is shown in (**Eq. 4**).

$$\boldsymbol{\Phi_D} = \begin{bmatrix} [1\ldots1] & 0 & 0 & 0 \\ 0 & [1\ldots1] & 0 & 0 \\ 0 & 0 & \ddots & 0 \\ 0 & 0 & 0 & [1\ldots1] \end{bmatrix} \tag{4}$$

The DBBD is a sparse matrix with each row having m = Z/M ones. ECG segments were compressed to 50% and 75% CRs, defined in (**Eq. 5**). CRs above 75% were not used as the reconstructed ECG had no discernable fiducial points. The uncompressed ECG segments will be considered compressed at 0% CR for the remainder of the paper. **Figure 2** shows an example of uncompressed and compressively sensed 10 s ECG. The amplification shown in the compressed ECG segments in **Figure 2** is due to the DBBD matrix and can be removed by normalizing the matrix, which does not have an impact on the proposed system nor the results presented.

$$\boldsymbol{C} = \left(1 - \frac{\boldsymbol{M}}{\boldsymbol{Z}}\right) * 100 \tag{5}$$

4.4 Training and Testing

A 10-fold record-based cross-validation (90%—training and 10%—testing) was used to test the proposed system. Record-based cross-validation is a cross-validation schema that isolates entire records for testing, such that the system was never trained and tested on ECG segments from the same record. The training procedure was divided into three main steps that were performed separately for each CR:

1) Train the SQI (Stage 1)
   a) Compressively sense the clean ECG records in the training set prior to corruption.
   b) Calculate the SD of the amplitudes.
   c) Extract the distribution of the amplitudes.
   d) Segment the ECG in the training set and corrupt the 30 s segments to the preset SNR range.
   e) Compressively sense the 30 s corrupted ECG segments.
   f) Calculate the ratios of the SDs of the amplitudes of the compressively sensed ECG segments and the SD of the clean ECG.
   g) Calculate the Wasserstein distance between the distributions of the amplitudes of the compressively sensed ECG segment and the distribution of the clean ECG.
   h) Train the Stage 1 RF.
2) Train the AF Detection in Compressively sensed ECG (Stage 2)
   a) Extract the features from the compressively sensed 30 s corrupted and clean ECG segments in the training set.
   b) Train the Stage 2 RF.
3) Train the AF Detection in Reconstructed ECG (Stage 3)
   a) Reconstruct the corrupted and clean compressively sensed ECG segments from the training set.
   b) Locate the R-waves and extract the RRIs.
   c) Extract the RRI features.
   d) Train the Stage 3 RF.

The testing procedure was also divided into three main steps that were performed separately for each CR:

1) Determine the SQI (Stage 1)
   a) Segment the ECG in the testing set and corrupt the 30 s segments to the preset SNR range.
   b) Compressively sense the 30 s corrupted ECG segments.
   c) Calculate the ratios of the SDs of the amplitudes of the uncompressed and compressively sensed ECG segments and the SD of the clean ECG calculated in step 1 (b) of the training procedure.
   d) Calculate the Wasserstein distance between the distributions of the amplitudes of the uncompressed and compressively sensed ECG segment and the distribution of the clean ECG extracted in step 1 (c) of the training procedure.
   e) Use the RF trained in step 1 (h) of the training procedure to determine the SQI of the ECG segment.
2) Detect AF in Compressively sensed ECG (Stage 2)
   a) Extract the features from the compressively sensed 30 s corrupted and clean ECG segments in the test set.
   b) Use the RF trained in step 2 (b) of the training procedure to classify the ECG segments as either N or AF and record the confidence score.
3) Detect AF in Reconstructed ECG (Stage 3)
   a) Reconstruct the compressively sensed 30 s corrupted and clean ECG segments in the test set.
   b) Locate the R waves and extract the RRIs.
   c) Extract the features.
   d) Use the RF trained in step 3 (d) of the training procedure to classify the ECG segments as either N or AF.

4.5 Evaluation

The performance of the system was evaluated using average precision (AP) [defined in (**Eq. 6**)], the area under the curve (AUC) of the receiver operator characteristic (ROC) curve, and F1-score [defined in (**Eq. 7**)]. In addition to AP, AUC, and F1 score, the system's true positive rate (TRP), false positive rate (FPR), and false discovery rate (FDR) were reported. The TPR is the rate of segments classified as AF over all AF segments. The FPR is the rate of segments misclassified as AF over all N segments. The FDR represents the false alarm rate and is the rate of segments misclassified as AF over all segments classified as AF.

$$\boldsymbol{AP} = \sum_{n=1}^{K} (\boldsymbol{R_n} - \boldsymbol{R_{n-1}})\boldsymbol{P_n} \tag{6}$$

where P_n is the precision at the nth confidence threshold, R_n is the recall at the nth threshold, and K is the number of the thresholds. The thresholds were between zero and one.

$$\boldsymbol{F1} = 2 * \frac{\boldsymbol{precision} * \boldsymbol{recall}}{\boldsymbol{precision} + \boldsymbol{recall}} \tag{7}$$

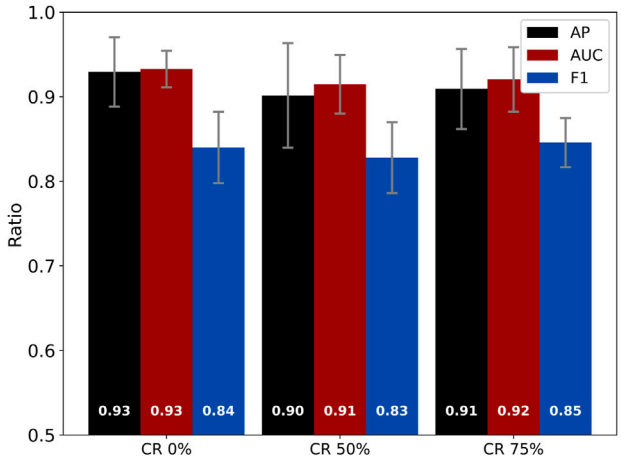

FIGURE 3 | Average precision, AUC, and F1 of Stage 2 across all CRs. The error bars are the SD of the results across the 10-fold record-based cross-validation.

TABLE 1 | Comparison of stage 2 performance with the literature.

Technique	CR (%)	Precision	Recall	F1 score	Accuracy
Stage 2 (Proposed)	50	1.00	0.92	0.96	0.97
	75	**1.00**	0.90	0.94	**0.97**
Poian et al. (2017)	50	0.97	0.85	N/A	0.93
	75	0.95	0.66	N/A	0.84
Cheng et al. (2020)	50	N/A	**0.96**	**0.97**	0.96
	70	N/A	0.95	0.96	0.94
Zhang et al. (2020)	50	0.96	0.95	0.95	0.95
	70	0.93	0.93	0.94	0.94

The bolded values are the maximum values in each column.

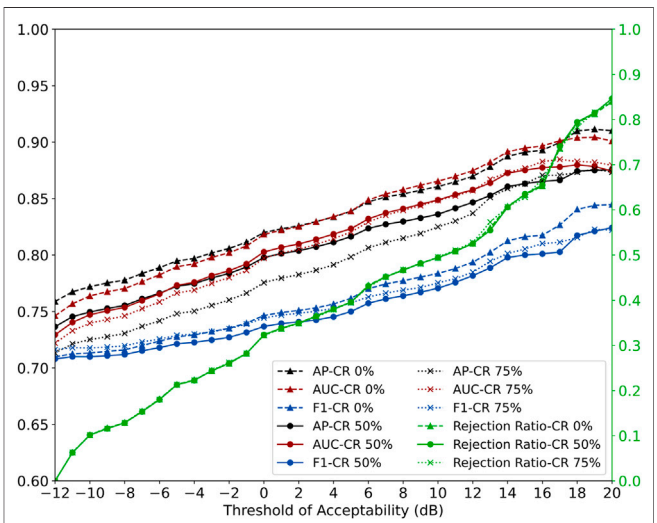

FIGURE 4 | AP, AUC, and F1, and rejection ratio of Stages 1 and 2 across all CRs using accepted segments only. The *x*-axis is the threshold of acceptability.

To compare with the literature the precision, recall, F1-score, and accuracy were calculated using segment-based hold-out method (90% training and 10% testing) on the AFDB, as this validation approach was used by the literature. Segment-based hold-out is a validation schema that divides the dataset into training and testing sets regardless of the source records, such that the training and testing segments may come from the same record.

The proposed system was tuned using the threshold of acceptability and the width of the unacceptable AF detection confidence range. The threshold of acceptability was placed on the SQI (Stage 1) to determine which ECG segments should be rejected. Thresholds between −12 and 20 dB were tested. A threshold of −12 dB would essentially accept all ECG segments. Thresholds above 20 dB rejected most of the test set, such that the performance of the system could not be evaluated. The system reported the rejection ratio (ratio of test segments rejected to the total number of test segments). During the evaluation of the system, rejecting a segment was considered the equivalent of classifying the segment as N.

The unacceptable AF detection confidence range was used to determine which ECG segments should be processed by Stage 3. The unacceptable AF detection confidence range was 0.1 wide, centered on 0.5. The width of the range was increased in steps of 0.05. For example, the first range was 0.45–0.55, such that ECG segments with Stage 2 AF detection confidence exclusively in that threshold range were processed by Stage 3. Segments above that range were classified as AF, and segments below were classified as N and bypassed Stage 3. The reconstruction ratio (ratio of reconstructed test segments to the total number of test segments) was reported.

The threshold of acceptability and the unacceptable confidence range were optimized using the Adaptive Geometry Estimation based Multi-objective Evolutionary Algorithm (AGE-MOE) (Panichella, 2019; Blank and Deb, 2020). The optimization was set as a minimization problem with the objectives being rejection ratio, reconstruction ratio, and 1-AP. The population size was 100, and the maximum number of generations was 30. The crossover and mutation were conducted using real simulated binary crossover and real polynomial mutation (Deb et al., 2007). The system was optimized for each CR, and the Pareto Fronts were used to demonstrate the relationship between the three objectives.

5 RESULTS

As a baseline, Stage 2 was tested on clean ECG segments. **Figure 3** shows AP, AUC, and F1 of Stage 2 across the CRs. The average AP, AUC, and F1 were 0.91, 0.92, and 0.84, respectively, across all CRs. **Table 1** summarizes the precision, recall, F1 score, and accuracy of Stage 2 and the literature. The quoted results in **Table 1** are based on segment-based hold-out method using the AFDB, since the literature used segment-based validation techniques as opposed to the record-based technique. The remainder of the results were generated using record-based cross-validation on the LTAFDB.

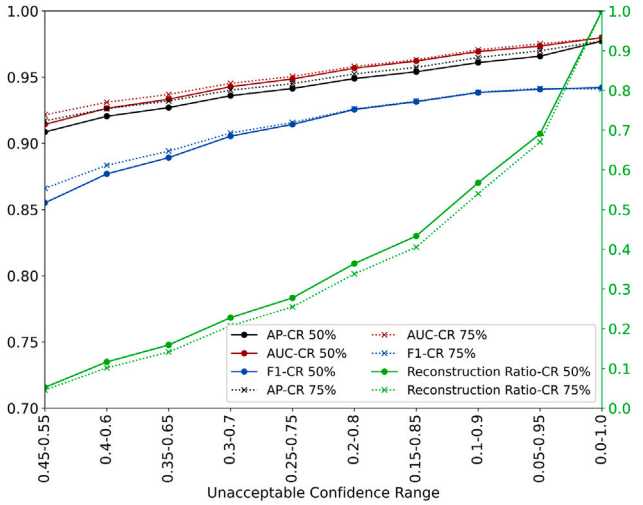

FIGURE 5 | AP, AUC, and F1, and reconstruction ratio of Stages 2 and 3 across 50% and 75% CRs on uncontaminated segments. The *x*-axis is the threshold of acceptable AF detection confidence.

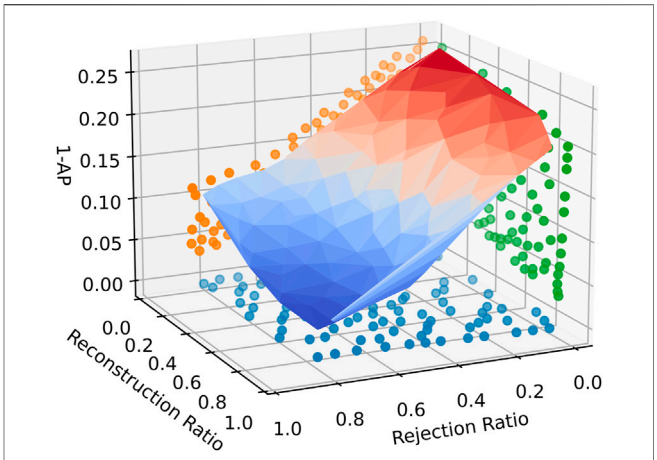

FIGURE 6 | The Pareto Front of the system optimized for 50% CR using accepted segments only. The color gradient represents the worst obtained AP (red) and the best AP (blue).

Stage 1 and Stage 2 were tested together to demonstrate the impact of the threshold of acceptability. **Figure 4** shows the AP, AUC, F1, and rejection ratio of Stages 1 and 2. At a threshold of acceptability of −12 dB, the rejection ratio is 0.00, and the system exhibits the lowest AP, AUC, and F1 (0.74, 0.73, and 0.71, respectively, averaged across all CRs). As the acceptability threshold increases, the AP, AUC, and F1 of the accepted segments improve, while more segments are rejected. At the highest threshold of acceptability (20 dB), the AP, AUC, and F1 are 0.88, 0.88, and 0.83, respectively, averaged across all CRs, and the average rejection ratio was 0.84.

Stage 2 and Stage 3 were tested together using clean ECG segments to demonstrate the impact of the unacceptable AF detection confidence range. **Figure 5** shows the AP, AUC, F1, and reconstruction ratio of Stages 2 and 3. For example, with the smallest unacceptable AF detection confidence range of 0.45–0.55, the reconstruction ratio is 0.05, and the system exhibits the same AP and AUC, and a 0.02 improvement in F1 (0.91, 0.92, and 0.86, respectively, averaged across all CRs) compared to Stage 2. As the unacceptable AF detection confidence range width increases, the AP, AUC, and F1 improve (at the range width of 0.50, reaching 0.98, 0.98, and 0.94, respectively, averaged across all CRs, where the average reconstruction ratio was 1.00).

The two parameters (threshold of acceptability and unacceptable AF detection confidence range) were optimized using AGE-MOE to obtain the Pareto Front (best set of results for a system). **Figure 6** shows the Pareto Front of the optimized system for the 50% CR. The Pareto Front of the 75% CR was almost identical. The color gradient represents the worst obtained AP (red) and the best AP (blue). The front is fairly linear with higher rejection and reconstruction ratios, resulting in higher AP.

TABLE 2 | Average execution time for each stage in the proposed system.

CR (%)	Stage 1 (ms)	Stage 2 (ms)	Stage 3
0	0.39	10.68	N/A
50	0.39	7.86	735.53 ms
75	0.39	6.62	369.50 ms

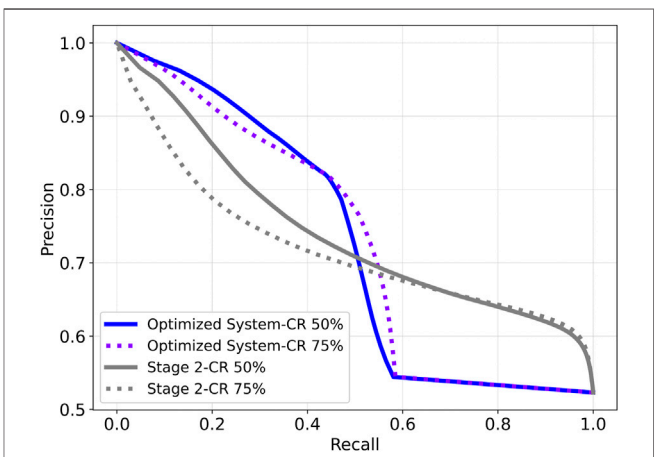

FIGURE 7 | Precision Recall Curve of the optimized system and Stage 2 for 50% and 75% CRs using contaminated segments.

Table 2 provides the average execution time for an ECG segment at each stage, running on an Intel Gold 6,148 Skylake. Stage 3 took approximately 93 times and 55 times longer to run than Stages 1 and 2 for 50% and 75% CRs, respectively, indicating that Stage 3 is computationally intensive.

An operating point was chosen that maximized the AP and minimized the reconstruction ratio. The chosen operating point for 50% CR was a 4 dB acceptability threshold and 0.30–0.70 threshold range of acceptable AF detection confidence, which

TABLE 3 | FPR, TPR, and FDR of different combinations of the stages and the optimized system.

CR (%)	Metric	Stage 2	Stage 3	Stage 1 + stage 2	Stage 1 + stage 3	Optimized system
50	TPR	0.79	0.44	0.46	0.42	0.45
	FPR	0.48	0.08	0.20	0.06	0.11
	FDR	0.36	0.14	0.28	0.12	0.19
75	TPR	0.81	0.51	0.46	0.44	0.47
	FPR	0.50	0.14	0.18	0.08	0.13
	FDR	0.36	0.20	0.27	0.14	0.20

TABLE 4 | TRP and FDR of different combinations of the stages and the optimized system at a FPR of 0.10.

CR (%)	Metric	Stage 2	Stage 3	Stage 1 + stage 2	Stage 1 + stage 3	Optimized system
50	TPR	0.33	0.45	0.34	0.45	0.43
	FDR	0.22	0.16	0.21	0.16	0.17
75	TPR	0.28	0.47	0.32	0.45	0.42
	FDR	0.25	0.16	0.20	0.16	0.17

resulted in 0.72 AP, 0.63 AUC, 0.58 F1, and 0.38 rejection and 0.38 reconstruction ratios. The chosen operating point for 75% CR was a 5 dB acceptability threshold and 0.30–0.70 threshold range of acceptable AF detection confidence, resulting in 0.72 AP, 0.63 AUC, 0.59 F1, and 0.40 rejection and 0.35 reconstruction ratios. **Figure 7** shows the precision-recall curve (PRC) of the optimized system and Stage 2. The maximum precision improvement of the optimized system over Stage 2 was 0.18 and 0.16 for 50% and 75% CRs, respectively, at recalls of 0.47 and 0.51, respectively. **Table 3** shows the TPR, FPR, FDR of the different combinations of the stages and the optimized system, and **Table 4** shows the TPR and FDR of the different combinations of the stages and the optimized system at an approximate FPR of 0.10.

6 DISCUSSION

The proposed system was tested using the LTAFDB to determine the performance in detecting AF in the compressively sensed ECG, the impact of rejecting corrupted ECG on the system's performance, and the impact of reconstructing the ECG to confirm the AF detection. AF detection with compressively sensed clean ECG (Stage 2) had an AP and AUC above 0.90, and F1 was above 0.83 (**Figure 3**), which was comparable to the results of the uncompressed case. The slight increase in the performance at the 75% CR was previously studied, and it was found that the filtering effects of the DBBD matrix aided in highlighting the features of AF (Abdelazez et al., 2021).

Poian et al. (2017), Cheng et al. (2020), and Zhang et al. (2020) developed an equivalent of Stage 2. At 50% and 75% CR, the proposed Stage 2 precision and accuracy were better than the literature (**Table 1**). On the other hand, the recall and F1 score of Cheng's technique were better than the proposed technique at both CRs. These results indicate that the proposed Stage 2 was comparable to the literature regardless of the compression ratio. It should be noted that the segment-based hold-out method approach reports inflated performance results. In a real-world scenario, an AF detection system would be trained on a set of patients and tested on another set with no mixing of segments from a single patient in both training and testing sets. **Table 1** reports the proposed system's segment-based hold-out results, since the literature reported results based on a similar validation schema.

The presence of contaminated ECG decreases the performance of the system. Generally, as the AP decreases, the false positives (i.e., false alarms) increase. In the context of remote monitoring, a high false alarm rate can render the system unusable. Using SQA to gate contaminated ECG with a threshold of acceptability can reduce the impact of contaminants (**Figure 4**); however, this is achieved at the expense of rejecting ECG segments, which may include rejecting ECG segments with AF (false negative). In practice, it would be reasonable not to raise an AF alarm when the ECG is contaminated, at which AF detection is difficult. Also, in long-term monitoring, the system can detect AF episodes in subsequent ECG segments, so a higher specificity can be used to justify a lower sensitivity. It is also noted that there were slight performance differences for Stage 1 between the different CRs.

In addition to rejecting corrupted ECG segments, the system's performance could be improved by selectively reconstructing ECG segments to detect AF (**Figure 5**); however, this is achieved at the cost of increased computation associated with reconstruction (**Table 2**). It should be noted that the values in **Table 2** were reported on a server-grade CPU with RAM available on demand. The computational time of each stage would most

likely be longer on an embedded device with limited resources. However, the ratio of the computational times of the different stages would be similar in an embedded device, assuming the embedded device has an architecture like that of server CPU (x86). As such, Stage 3 would still be the most computationally time-consuming stage on an embedded device. The relationships between the AP, AUC, F1, reconstruction ratio, and the threshold range width were pretty linear, except for the highest threshold range widths. Above the threshold range 0.15–0.85, the reconstruction ratio increased exponentially, while the AP, AUC, and F1 began to plateau as they approached the performance of AF detection in uncompressed ECG using the RRI features. The performance of Stage 3 was similar across the different CRs. It should be noted that the chosen unacceptable confidence range was symmetrical around 0.5 to improve both precision (i.e., reduce false alarms) and recall (i.e., reduce missed alarms). However, if the goal is only to reduce false alarms, a non-symmetrical range could have been used. For example, the lower end of the threshold range could have been fixed at 0.5, so segments classified as N would be accepted as such, regardless of the confidence in the classification. The advantage of using a non-symmetrical unacceptable confidence range is the reduction of the usage of the computationally intensive Stage 3.

The Pareto Front of the optimized system (**Figure 6**) shows that the relationship between the AP and reconstruction and rejection ratios is fairly linear. The PRC (**Figure 7**) of 50% and 75% CRs were similar, with the 75% CR having slightly better precision than 50% CR at higher CRs due to the filtering effect of the DBBD. Since the objective was to reduce false alarms, the system was optimized to improve precision at the recall's expense. The PRC of the optimized system was better than Stage 2 up to recall of 0.50 and 0.55 (50% and 75 CRs, respectively), beyond which the PRC dropped below Stage 2. The optimized system improved precision up to 0.18, which resulted in low false alarms.

The optimized system reduced the FPR by 0.37 and FDR by 0.17 and 0.16 at 50% and 75% CRs, respectively (**Table 3**). Stage 2 had high TPR, FPR, and FDR, while Stage 3 had low TPR, FPR, and FDR. When using Stage 1, to reject low-quality ECG segments, with Stage 2, the FPR and FDR were reduced by over 0.28 and 0.08, respectively, when compared to Stage 2 alone. On the other hand, rejecting low-quality ECG (Stage 1) with Stage 3 had minimal impact on the FPR and the FDR. Stage 3 had low FPR and FDR, indicating that the low-quality segments were classified as N. As such, using Stage 1 to reject low-quality ECG had minimal impact on the number of false positives hence the minimal impact on FPR and FDR. The optimized system leverages Stage 2 high TPR and Stage 3 low FPR and FDR. As a result, the system had a TPR comparable to Stage 2 with Stage 1 high TPR while having slightly worse FPR and FDR than Stage 3 with Stage 1.

The probability of false alarms (i.e., FPR) could be set to a specific rate that the users are tolerant to in a real-world application. At a FPR of 0.10, the optimized system had a TPR of 0.43 and 0.42 and an FDR of 0.17 for 50% and 75% CRs, respectively (**Table 4**). The optimized system had TPR 0.10 and 0.14 more than the TPR of Stage 2 alone and FDR 0.05 and 0.08 less than the FDR of Stage 2 alone. The improvements in the TPR and FDR were mainly due to Stage 3, where the TPR was 0.45 and FDR was 0.16 for 50% and 75% CRs. Stage 1 had minimal impact on the TPR and FDR since the FPR was manually set to a certain level. **Table 4** also showed that reconstructing all the ECG only had a 0.02 and 0.03 TPR improvement and 0.01 FDR improvement over the optimized system, which only had a reconstruction ratio below 0.38. Considering that 50% and 75% CRs had similar PRCs, a difference of 0.01 in their TPRs and no difference in their FDRs, a CR of 75% provided the best performance while maximizing compression, which can reduce the power consumption of a remote wearable ECG monitor.

The proposed system demonstrated that AF could be detected in compressively sensed ECG while reducing false alarms and ECG reconstruction. However, there are limitations and areas of improvement in the system. The system was validated on a single lead from a single database that had 89 subjects that were contaminated with motion artifact only. The TPR of the optimized system was 0.45 and 0.47 for 50% and 75% CRs, respectively, and even though in long-term monitoring, a missed alarm could be identified later, the TPR could be further improved. Another limitation of the proposed system is the presence of other cardiovascular diseases that may resemble AF as the training and testing did not consider these diseases and only used a N and AF rhythms.

7 CONCLUSION

A system was proposed to detect AF in compressively sensed ECG while minimizing false alarms due to contaminated ECG and ECG reconstruction. The system detected AF in compressively sensed ECG with minimal performance degradation compared to detection of AF in uncompressed ECG. Contaminated ECG decreased the performance of the AF detection; however, the proposed gating (Stage 1) and selective reconstruction (Stage 3) improved the system's performance in the presence of contaminated ECG.

Future work will explore the system's adaptability to a different Stage 2 (e.g., Poian's technique), the detection of AF in the presence of other cardiovascular diseases, and the impact of contamination other than motion artifact on the system performance. Additionally, a privacy-preserving sensing matrix that highlights AF features will be explored.

DATA AVAILABILITY STATEMENT

Publicly available datasets were analyzed in this study. This data can be found here: https://physionet.org/content/ltafdb/1.0.0/, https://physionet.org/content/afdb/1.0.0/.

ETHICS STATEMENT

Ethical review and approval was not required for the study on human participants in accordance with the local legislation and institutional requirements. Written informed consent for

participation was not required for this study in accordance with the national legislation and the institutional requirements.

AUTHOR CONTRIBUTIONS

MA developed the methods and wrote the manuscript under the supervision of SR and AC.

ACKNOWLEDGMENTS

The authors would like to acknowledge Canada's Natural Sciences and Engineering Research Council for supporting this research through their Discovery Grant, CREATE-BEST, and Vanier scholarships. In addition, this research was enabled in part by support provided by Calcul Québec (www.calculquebec.ca) and Compute Canada (www.computecanada.ca).

REFERENCES

Abdelazez, M., Quesnel, P. X., Chan, A. D. C., and Yang, H. (2017). Signal Quality Analysis of Ambulatory Electrocardiograms to Gate False Myocardial Ischemia Alarms. *IEEE Trans. Biomed. Eng.* 64, 1318–1325. doi:10.1109/TBME.2016.2602283

Abdelazez, M., Firouzeh, F. F., Rajan, S., and Chan, A. D. C. (2020). "Multi-Stage Detection of Atrial Fibrillation in Compressively Sensed Electrocardiogram," in 2020 IEEE International Instrumentation and Measurement Technology Conference (I2MTC), Dubrovnik, Croatia, 1–6. doi:10.1109/I2MTC43012.2020.9128396

Abdelazez, M., Rajan, S., and Chan, A. D. C. (2021). Detection of Atrial Fibrillation in Compressively Sensed Electrocardiogram Measurements. *IEEE Trans. Instrum. Meas.* 70, 1–9. doi:10.1109/TIM.2020.3027930

Abdelazez, M., Rajan, S., and Chan, A. D. C. (2022). Signal Quality Assessment of Compressively Sensed Electrocardiogram. *IEEE Trans. Biomed. Eng.*, 1. doi:10.1109/TBME.2022.3170047

Al Disi, M., Djelouat, H., Kotroni, C., Politis, E., Amira, A., Bensaali, F., et al. (2018). ECG Signal Reconstruction on the IoT-Gateway and Efficacy of Compressive Sensing under Real-Time Constraints. *IEEE Access* 6, 69130–69140. doi:10.1109/ACCESS.2018.2877679

Alonso, A., Agarwal, S. K., Soliman, E. Z., Ambrose, M., Chamberlain, A. M., Prineas, R. J., et al. (2009). Incidence of Atrial Fibrillation in Whites and African-Americans: The Atherosclerosis Risk in Communities (ARIC) Study. *Am. Heart J.* 158, 111–117. doi:10.1016/j.ahj.2009.05.010

Andersen, R. S., Peimankar, A., and Puthusserypady, S. (2019). A Deep Learning Approach for Real-Time Detection of Atrial Fibrillation. *Expert Syst. Appl.* 115, 465–473. doi:10.1016/j.eswa.2018.08.011

Asgari, S., Mehrnia, A., and Moussavi, M. (2015). Automatic Detection of Atrial Fibrillation Using Stationary Wavelet Transform and Support Vector Machine. *Comput. Biol. Med.* 60, 132–142. doi:10.1016/j.compbiomed.2015.03.005

Bashar, S. K., Hossain, M.-B., Lázaro, J., Ding, E. Y., Noh, Y., Cho, C. H., et al. (2021). Feasibility of Atrial Fibrillation Detection from a Novel Wearable Armband Device. *Cardiovasc. Digit. Health J.* 2, 179–191. doi:10.1016/j.cvdhj.2021.05.004

Blank, J., and Deb, K. (2020). Pymoo: Multi-Objective Optimization in Python. *IEEE Access* 8, 89497–89509. doi:10.1109/ACCESS.2020.2990567

Candès, E. J., Romberg, J. K., and Tao, T. (2006). Stable Signal Recovery from Incomplete and Inaccurate Measurements. *Commun. Pure Appl. Math.* 59, 1207–1223. doi:10.1002/cpa.20124

Cheng, Y., Hu, Y., Hou, M., Pan, T., He, W., and Ye, Y. (2020). Atrial Fibrillation Detection Directly from Compressed ECG with the Prior of Measurement Matrix. *Information* 11, 436. doi:10.3390/info11090436

Couderc, J.-P., Kyal, S., Mestha, L. K., Xu, B., Peterson, D. R., Xia, X., et al. (2015). Detection of Atrial Fibrillation Using Contactless Facial Video Monitoring. *Heart rhythm.*. 12, 195–201. doi:10.1016/j.hrthm.2014.08.035

Deb, K., Sindhya, K., and Okabe, T. (2007). "Self-adaptive Simulated Binary Crossover for Real-Parameter Optimization," in Proceedings of the 9th annual conference on Genetic and evolutionary computation GECCO '07 (New York, NY, USA: Association for Computing Machinery), 1187–1194. doi:10.1145/1276958.1277190

Donoho, D. L. (2006). Compressed Sensing. *IEEE Trans. Inf. Theory* 52, 1289–1306. doi:10.1109/TIT.2006.871582

Farago, E., and Chan, A. D. C. (2020). "Simulating Motion Artifact Using an Autoregressive Model for Research in Biomedical Signal Quality Analysis," in 2020 42nd Annual International Conference of the IEEE Engineering in Medicine Biology Society (EMBC), Montreal, Canada, 940–943. doi:10.1109/EMBC44109.2020.9175965

Fraser, G. D., Chan, A. D. C., Green, J. R., and MacIsaac, D. T. (2014). Automated Biosignal Quality Analysis for Electromyography Using a One-Class Support Vector Machine. *IEEE Trans. Instrum. Meas.* 63, 2919–2930. doi:10.1109/TIM.2014.2317296

Go, A. S., Mozaffarian, D., Roger, V. L., Benjamin, E. J., Berry, J. D., Blaha, M. J., et al. (2014). Heart Disease and Stroke Statistics—2014 Update A Report from the American Heart Association. *Circulation* 129, e28–e292. doi:10.1161/01.cir.0000441139.02102.80

Goldberger, A. L., Amaral, L. A. N., Glass, L., Hausdorff, J. M., Ivanov, P. C., Mark, R. G., et al. (2000). PhysioBank, PhysioToolkit, and PhysioNet Components of a New Research Resource for Complex Physiologic Signals. *Circulation* 101, e215–e220. doi:10.1161/01.CIR.101.23.e215

Han, D., Bashar, S. K., Zieneddin, F., Ding, E., Whitcomb, C., McManus, D. D., et al. (2020). "Digital Image Processing Features of Smartwatch Photoplethysmography for Cardiac Arrhythmia Detection," in 2020 42nd Annual International Conference of the IEEE Engineering in Medicine and Biology Society (EMBC) in conjunction with the 43rd Annual Conference of the Canadian Medical and Biological Engineering Society, Montreal, Canada, 4071–4074. doi:10.1109/EMBC44109.2020.9176142

Hussein, A. F., kumar, N. A., Burbano-Fernandez, M., Ramírez-González, G., Abdulhay, E., and De Albuquerque, V. H. C. (2018). An Automated Remote Cloud-Based Heart Rate Variability Monitoring System. *IEEE Access* 6, 77055–77064. doi:10.1109/ACCESS.2018.2831209

January, C. T., Wann, L. S., Alpert, J. S., Calkins, H., Cigarroa, J. E., Conti, J. B., et al. (2014). 2014 AHA/ACC/HRS Guideline for the Management of Patients with Atrial Fibrillation: a Report of the American College of Cardiology/American Heart Association Task Force on Practice Guidelines and the Heart Rhythm Society. *J. Am. Coll. Cardiol.* 64, e1–e76. doi:10.1016/j.jacc.2014.03.022

Kannel, W. B., Wolf, P. A., Benjamin, E. J., and Levy, D. (1998). Prevalence, Incidence, Prognosis, and Predisposing Conditions for Atrial Fibrillation: Population-Based Estimates 11Reprints Are Not Available. *Am. J. Cardiol.* 82, 2N–9N. doi:10.1016/S0002-9149(98)00583-9

Kligfield, P., Gettes, L. S., Bailey, J. J., Childers, R., Deal, B. J., Hancock, E. W., et al. (2007). Recommendations for the Standardization and Interpretation of the Electrocardiogram. *J. Am. Coll. Cardiol.* 49, 1109–1127. doi:10.1016/j.jacc.2007.01.024

Kora, P., and Sri Rama Krishna, K. (2016). ECG Based Heart Arrhythmia Detection Using Wavelet Coherence and Bat Algorithm. *Sens. Imaging* 17, 12. doi:10.1007/s11220-016-0136-5

Kumar Sahoo, S., Lu, W., Teddy, S. D., Kim, D., and Feng, M. (2011). "Detection of Atrial Fibrillation from Non-episodic ECG Data: A Review of Methods," in 2011 Annual International Conference of the IEEE Engineering in Medicine and Biology Society (Boston, MA: IEEE), 4992–4995. doi:10.1109/IEMBS.2011.6091237

Kusumoto Fred, M., Schoenfeld Mark, H., Barrett, C., Edgerton James, R., Ellenbogen Kenneth, A., Gold, M. R., et al. (2019). 2018 ACC/AHA/HRS Guideline on the Evaluation and Management of Patients with Bradycardia and Cardiac Conduction Delay: A Report of the American College of Cardiology/American Heart Association Task Force on Clinical Practice Guidelines and the Heart Rhythm Society. *Circulation* 140, e382–e482. doi:10.1161/CIR.0000000000000628

Lazaro, J., Reljin, N., Hossain, M.-B., Noh, Y., Laguna, P., and Chon, K. H. (2020). Wearable Armband Device for Daily Life Electrocardiogram Monitoring. *IEEE Trans. Biomed. Eng.* 67, 3464–3473. doi:10.1109/TBME.2020.2987759

Lim, H. W., Hau, Y. W., Lim, C. W., and Othman, M. A. (2016). Artificial Intelligence Classification Methods of Atrial Fibrillation with Implementation Technology. *Comput. Assist. Surg.* 21, 154–161. doi:10.1080/24699322.2016.1240303

Lin, C.-H. (2008). Frequency-domain Features for ECG Beat Discrimination Using Grey Relational Analysis-Based Classifier. *Comput. Math. Appl.* 55, 680–690. doi:10.1016/j.camwa.2007.04.035

Liu, J., Xu, W., Zhao, P., and Hua, J. (2021). A Signal Quality Analysis Method for Electrocardiosignals in the CS Domain. *Meas. Sci. Technol.* 32, 095116. doi:10.1088/1361-6501/abf176

Maji, U., Mitra, M., and Pal, S. (2013). Automatic Detection of Atrial Fibrillation Using Empirical Mode Decomposition and Statistical Approach. *Procedia Technol.* 10, 45–52. doi:10.1016/j.protcy.2013.12.335

Marinho, L. B., Nascimento, N. de M. M., Souza, J. W. M., Gurgel, M. V., Rebouças Filho, P. P., and de Albuquerque, V. H. C. (2019). A Novel Electrocardiogram Feature Extraction Approach for Cardiac Arrhythmia Classification. *Future Gener. Comput. Syst.* 97, 564–577. doi:10.1016/j.future.2019.03.025

Martis, R. J., Acharya, U. R., Adeli, H., Prasad, H., Tan, J. H., Chua, K. C., et al. (2014). Computer Aided Diagnosis of Atrial Arrhythmia Using Dimensionality Reduction Methods on Transform Domain Representation. *Biomed. Signal Process. Control* 13, 295–305. doi:10.1016/j.bspc.2014.04.001

Medtronic (2020). Medtronic Cardiac Monitors - Reveal LINQ ICM System. Available at: https://europe.medtronic.com/xd-en/healthcare-professionals/products/cardiac-rhythm/cardiac-monitors/reveal-linq-icm.html (Accessed June 3, 2020).

Mitra, D., Zanddizari, H., and Rajan, S. (2020). Investigation of Kronecker-Based Recovery of Compressed ECG Signal. *IEEE Trans. Instrum. Meas.* 69, 3642–3653. doi:10.1109/TIM.2019.2936776

Mohimani, H., Babaie-Zadeh, M., and Jutten, C. (2009). A Fast Approach for Overcomplete Sparse Decomposition Based on Smoothed Sl0 Norm. *IEEE Trans. Signal Process.* 57, 289–301. doi:10.1109/TSP.2008.2007606

Moody, G. B., Muldrow, W., and Mark, R. G. (1984). A Noise Stress Test for Arrhythmia Detectors. *Comput. Cardiol.* 11, 381–384.

Moody, G. (1983). A New Method for Detecting Atrial Fibrillation Using RR Intervals. *Comput. Cardiol.*, 227–230.

Mousavi, S., Afghah, F., Razi, A., and Acharya, U. R. (2019). "ECGNET: Learning where to Attend for Detection of Atrial Fibrillation with Deep Visual Attention," in 2019 IEEE EMBS International Conference on Biomedical Health Informatics (BHI), 1–4. doi:10.1109/BHI.2019.8834637

Nascimento, N. M. M., Marinho, L. B., Peixoto, S. A., do Vale Madeiro, J. P., de Albuquerque, V. H. C., and Filho, P. P. R. (2020). Heart Arrhythmia Classification Based on Statistical Moments and Structural Co-occurrence. *Circuits Syst. Signal Process.* 39, 631–650. doi:10.1007/s00034-019-01196-w

Ott, A., Breteler, M. M. B., Bruyne, M. C. d., Harskamp, F. v., Grobbee, D. E., and Hofman, A. (1997). Atrial Fibrillation and Dementia in a Population-Based Study. *Stroke* 28, 316–321. (Accessed September 27, 2018). doi:10.1161/01.str.28.2.316

Pan, J., and Tompkins, W. J. (1985). A Real-Time QRS Detection Algorithm. *IEEE Trans. Biomed. Eng.* 32, 230–236. doi:10.1109/tbme.1985.325532

Panichella, A. (2019). "An Adaptive Evolutionary Algorithm Based on Non-euclidean Geometry for Many-Objective Optimization," in Proceedings of the Genetic and Evolutionary Computation Conference GECCO '19 (New York, NY, USA: Association for Computing Machinery), 595–603. doi:10.1145/3321707.3321839

Pereira, T., Tran, N., Gadhoumi, K., Pelter, M. M., Do, D. H., Lee, R. J., et al. (2020). Photoplethysmography Based Atrial Fibrillation Detection: a Review. *Npj Digit. Med.* 3, 1–12. doi:10.1038/s41746-019-0207-9

Petrutiu, S., Sahakian, A. V., and Swiryn, S. (2007). Abrupt Changes in Fibrillatory Wave Characteristics at the Termination of Paroxysmal Atrial Fibrillation in Humans. *EP Eur.* 9, 466–470. doi:10.1093/europace/eum096

Podd, S. J., Sugihara, C., Furniss, S. S., and Sulke, N. (2016). Are Implantable Cardiac Monitors the 'gold Standard' for Atrial Fibrillation Detection? A Prospective Randomized Trial Comparing Atrial Fibrillation Monitoring Using Implantable Cardiac Monitors and DDDRP Permanent Pacemakers in Post Atrial Fibrillation Ablation Patients. *EP Eur.* 18, 1000–1005. doi:10.1093/europace/euv367

Poian, G. D., Brandalise, D., Bernardini, R., and Rinaldo, R. (2016). Energy and Quality Evaluation for Compressive Sensing of Fetal Electrocardiogram Signals. *Sensors* 17, 9. doi:10.3390/s17010009

Poian, G. D., Liu, C., Bernardini, R., Rinaldo, R., and Clifford, G. D. (2017). Atrial Fibrillation Detection on Compressed Sensed ECG. *Physiol. Meas.* 38, 1405–1425. doi:10.1088/1361-6579/aa7652

Poian, G. D., Rozell, C. J., Bernardini, R., Rinaldo, R., and Clifford, G. D. (2018). Matched Filtering for Heart Rate Estimation on Compressive Sensing ECG Measurements. *IEEE Trans. Biomed. Eng.* 65, 1349–1358. doi:10.1109/TBME.2017.2752422

Pokaprakarn, T., Kitzmiller, R. R., Moorman, R., Lake, D. E., Krishnamurthy, A. K., and Kosorok, M. (2021). Sequence to Sequence ECG Cardiac Rhythm Classification Using Convolutional Recurrent Neural Networks. *IEEE J. Biomed. Health Inf.* 26, 572–581. doi:10.1109/JBHI.2021.3098662

Qiao Li, Q. L., Chengyu Liu, C. L., Oster, J. O., and Clifford, G. D. C. (2016). "Signal Processing and Feature Selection Preprocessing for Classification in Noisy Healthcare Data," in *Machine Learning for Healthcare Technologies*. Editor D. A. C. Clifton (Institution of Engineering and Technology), 33–58. doi:10.1049/PBHE002E_ch3

Quesnel, P. X., Chan, A. D., and Yang, H. (2014). "Signal Quality and False Myocardial Ischemia Alarms in Ambulatory Electrocardiograms," in 2014 IEEE International Symposium on Medical Measurements and Applications (MeMeA) (IEEE), 1–5. Available at: http://ieeexplore.ieee.org/xpls/abs_all.jsp?arnumber=6860078. (Accessed August 5, 2016). doi:10.1109/memea.2014.6860078

Reiffel, J. A., Verma, A., Kowey, P. R., Halperin, J. L., Gersh, B. J., Wachter, R., et al. (2017). Incidence of Previously Undiagnosed Atrial Fibrillation Using Insertable Cardiac Monitors in a High-Risk Population: The REVEAL AF Study. *JAMA Cardiol.* 2, 1120–1127. doi:10.1001/jamacardio.2017.3180

Rizwan, A., Zoha, A., Mabrouk, I., Sabbour, H., Al-Sumaiti, A., Alomaniy, A., et al. (2020). A Review on the State of the Art in Atrial Fibrillation Detection Enabled by Machine Learning. *IEEE Rev. Biomed. Eng.* 14, 219–239. doi:10.1109/RBME.2020.2976507

Satija, U., Ramkumar, B., and Manikandan, M. S. (2018). A Review of Signal Processing Techniques for Electrocardiogram Signal Quality Assessment. *IEEE Rev. Biomed. Eng.* 11, 36–52. doi:10.1109/RBME.2018.2810957

Scott, D. W. (2011). "Sturges' and Scott's Rules," in *International Encyclopedia of Statistical Science*. Editor M. Lovric (Berlin, Heidelberg: Springer), 1563–1566. doi:10.1007/978-3-642-04898-2_578

Sedghamiz, H. (2014). *Complete Pan Tompkins Implementation ECG QRS Detector*. Sweden: Linkoping University.

Serhani, M. A., El Kassabi, T. H., Ismail, H., and Nujum Navaz, A. (2020). ECG Monitoring Systems: Review, Architecture, Processes, and Key Challenges. *Sensors* 20, 1796. doi:10.3390/s20061796

Stewart, S., Hart, C. L., Hole, D. J., and McMurray, J. J. V. (2002). A Population-Based Study of the Long-Term Risks Associated with Atrial Fibrillation: 20-year Follow-Up of the Renfrew/Paisley Study. *Am. J. Med.* 113, 359–364. doi:10.1016/S0002-9343(02)01236-6

Sun, L., Wang, Y., He, J., Li, H., Peng, D., and Wang, Y. (2020). A Stacked LSTM for Atrial Fibrillation Prediction Based on Multivariate ECGs. *Health Inf. Sci. Syst.* 8, 19. doi:10.1007/s13755-020-00103-x

Taji, B., Chan, A. D. C., and Shirmohammadi, S. (2018). False Alarm Reduction in Atrial Fibrillation Detection Using Deep Belief Networks. *IEEE Trans. Instrum. Meas.* 67, 1124–1131. doi:10.1109/TIM.2017.2769198

Villani, C. (2009). "The Wasserstein Distances," in *Optimal Transport: Old and New*. Editor C. Villani (Berlin, Heidelberg: Springer), 93–111. Grundlehren der Mathematischen Wissenschaften. doi:10.1007/978-3-540-71050-9_6

Zhang, H., Dong, Z., Gao, J., Lu, P., and Wang, Z. (2020). Automatic Screening Method for Atrial Fibrillation Based on Lossy Compression of the Electrocardiogram Signal. *Physiol. Meas.* 41, 075005. doi:10.1088/1361-6579/ab979f

Conflict of Interest: The authors declare that the research was conducted in the absence of any commercial or financial relationships that could be construed as a potential conflict of interest.

Publisher's Note: All claims expressed in this article are solely those of the authors and do not necessarily represent those of their affiliated organizations, or those of the publisher, the editors and the reviewers. Any product that may be evaluated in this article, or claim that may be made by its manufacturer, is not guaranteed or endorsed by the publisher.